Catal Lett (2009) 127:248–259
DOI 10.1007/s10562-008-9748-2

Characterizing $Hf_XZr_{1-X}O_2$ by EXAFS: Relationship Between Bulk and Surface Composition, and Impact on Catalytic Selectivity for Alcohol Conversion

Gary Jacobs · Mark Milling · Yaying Ji · Patricia M. Patterson · Dennis E. Sparks · Burtron H. Davis

Received: 22 August 2008 / Accepted: 23 October 2008 / Published online: 11 November 2008

Abstract A series of mixed $Hf_XZr_{1-X}O_2$ oxide catalysts was prepared according to a recipe that yields the monoclinic structure. The samples were examined by EXAFS spectroscopy at the Zr K and Hf L_{III} edges. A fitting model was used that simultaneously fits data from both edges, and makes use of an interdependent mixing parameter X_{mix} to take into account substitution of the complementary atom in the nearest metal-metal shell. For XPS analysis, Scofield factors were applied to estimate the relative atomic surface concentrations of Zr and Hf. EXAFS results suggested that a solid bulk solution was formed over a wide range of X for $Hf_XZr_{1-X}O_2$ binary oxides, and that the relative ratio was retained in the surface shell (i.e., including some subsurface layers by XPS) and the surface (e.g., by ISS). The increase in selectivity for the 1-alkene from dehydration of alcohols at high Zr content does not correlate smoothly with the tuned relative atomic concentration of Hf to Zr. The step change at high Zr content appears to be due to other indirect factors (e.g., surface defects, oxygen vacancies).

Keywords Hafnia · Zirconia · Binary mixed oxide · Homogeneous solid solution · Homogeneity · EXAFS · XPS · Dehydrogenation · Dehydration · Alcohols · Butanol · Octanol

G. Jacobs · M. Milling · Y. Ji · P. M. Patterson · D. E. Sparks · B. H. Davis (✉)
Center for Applied Energy Research, University of Kentucky, 2540 Research Park Dr., Lexington, KY 40511, USA
e-mail: davis@caer.uky.edu

1 Introduction

Binary oxides have been reported to offer many distinct advantages in heterogeneous catalysis over single oxide materials. One important system that has been well studied is that of ceria and zirconia. Some benefits that have been reported include (a) enhanced oxygen mobility and transfer rates [1–3], (b) enhanced oxygen storage capacity [4, 5], (c) enhanced decomposition rates for certain species, such as carbonates during water gas shift [6, 7], and (d) improved structural integrity resulting in stabilization of the oxide surface area [8], resulting in a potentially lower deactivation rate for a host of reactions.

In moving to mixed oxides, additional parameters come into play to describe the increased complexity of the system. The most obvious is that of oxide homogeneity [1, 9]. Others include the strain on the crystallite structure introduced by the dopant [10], the static disorder arising from defects in the structure, changes in the acid-base characteristics (e.g., number and strength of acid/basic sites) on the catalyst surface [10], and changes in the electronic properties [11]. These properties can, in turn, influence the mobility of atoms (e.g., oxygen) within the bulk of the solid as well as at the surface. As such, the reduction property of the bulk and the surface (e.g., temperature and extent) can also be improved [1, 7, 12, 13].

The aim of this contribution was to explore the potential of employing EXAFS to obtain meaningful information on binary oxide catalysts, with a focus on bulk properties such as degree of mixing at the local atomic level and therefore, solid oxide solution homogeneity. In order to assess its potential usage, we sought a system that had already been well-characterized and moreover, should exhibit almost perfect mixing—hafnia and zirconia. The heats of formation of hafnia and zirconia are nearly the same, so that there

should not be a strong driving force for surface enrichment by one particular metal [14]. To determine whether or not the bulk composition determined by EXAFS could be extrapolated to the surface, XPS was employed to assess the surface shell ratio of Hf to Zr. Since at the required energies, XPS also yields photoelectrons from subsurface layers in addition to the surface, the results from XPS were compared with our previous results of ISS [15]. Indeed, in past studies employing X-ray diffraction and Raman spectroscopy, the catalysts characterized in this work were strongly suggested to exhibit surface compositions that were virtually identical to the bulk [16].

Another driving force for the determination of bulk and surface composition relates to catalytic selectivity during alcohol conversion. Freeman et al. [17] noted, for example, that the 1-alkene selectivity for 2-octanol dehydration by zirconia was markedly higher than that of hafnia.

However, in attempts to tune catalytic selectivity based on adjusting the composition, it has been observed that, in lieu of a smooth change in selectivity, a step change occurred at a concentration of ~75 mol% zirconia over a series of solid monoclinic solutions. For catalysts prepared in a different manner, in which hafnia was doped into the surface layer of zirconia, a step change was also observed, albeit at ~90 mol% zirconia. Likewise, a similar finding was obtained with the analog 2-butanol for the hafnia doped zirconia sample. At ~90 mol% zirconia, the selectivity to dehydration increased by a step-change.

The use of EXAFS and XPS was therefore important to provide a check on earlier results as to whether or not surface-enrichment occurred.

2 Experimental

2.1 Catalyst Preparation

Zirconia was prepared by rapidly adding excess concentrated ammonium hydroxide into a vigorously stirred 0.3 M aqueous solution of zirconyl nitrate. The precipitate was subsequently filtered, washed, dried, and calcined in a muffle furnace at 600 °C [16].

Hafnium metal was first dissolved in aqueous hydrofluoric acid and then ammonium hydroxide was added to effect precipitation of the hydrous oxide. The gel was washed five times by repeated dispersion and filtration steps. The washed gel was then dissolved in concentrated nitric acid. An appropriate amount of this Hf solution was added to a zirconyl nitrate solution to provide the desired Hf–Zr concentration. A mixed metal gel was prepared by precipitation by adding concentrated ammonia. The gel was dried and calcined in a manner similar to that for the undoped zirconia sample.

For comparative purposes, hafnium doped zirconia catalysts were also prepared. Monoclinic zirconia was impregnated with an appropriate amount of hafnium nitrate solution (described above). The amount of hafnium required to give the desired surface coverage was calculated assuming that hafnia occupied an area corresponding to the area projected onto a base plane of the hafnia unit cell. The impregnated material was dried at 120 °C and calcined at 600 °C in air.

2.2 X-ray Photoelectron Spectroscopy

XPS experiments were carried out using a Thermo VG Scientific Minilab. Mg Kα X-rays (Kinetic energy 1273 eV) were used with a dual cathode X-ray gun. The pressure in the analysis chamber was between 9 and 5 E−10 Torr. Data were collected using a hemispherical electron analyzer.

Spectra were first baseline corrected. Then, areas of peaks for the Zr 3d, Hf 4f, and O 1s ionizations were determined, and Scofield factors [18] were applied to convert the intensities to atomic surface concentrations. In this manner, the Zr/(Zr + Hf) ratio could be ascertained for each binary oxide sample. The spectra were normalized by the combined adjusted areas of the Zr, Hf, and O signals, so that the spectra could be compared graphically. Binding energy shifts were corrected by analyzing the shift in the C 1s signal for each catalyst sample.

2.3 Extended X-ray Absorption Fine Structure Spectroscopy

EXAFS spectra were recorded at the Hf L_{III} and Zr K edges at Beamline X-18b at the National Synchrotron Light Source (NSLS) at Brookhaven National Laboratory (BNL) in Upton, New York. The beamline parameters and crystal detuning procedure have been previously reported [19].

It was imperative for these binary oxide catalysts to first calculate sample thicknesses prior to visiting the synchrotron. We calculated sample thicknesses by determining the amount of sample ω_D, in grams per square centimeter, using the thickness equation:

$$\omega_D = \ln(I_0/I_t) \Big/ \sum (\mu/\rho)_j w_j,$$

where μ/ρ is the total absorption cross section of element j in the sample at the absorption edge of the EXAFS element under study in cm^3/g, w_j is the weight fraction of element j in the sample, and $\ln(I_0/I_t)$ was taken over a typical range of 1–2.5. Using the calculation for ω_D, along with the cross-sectional area of the wafer, the mass of the sample was obtained. To produce a pinhole-free, self-supporting wafer, BN was used to dilute the catalyst sample. Samples

were scanned in flowing helium (500 cm^3/min) at the boiling temperature of liquid nitrogen to minimize the dynamic component in the Debye-Waller factors. The use of helium was a precautionary measure to prevent ice formation within the cell. Scans were carried out in transmission mode. WinXAS [20] was employed to carry out standard data reduction, including edge calibration, background subtraction and normalization (two-polynomial method with degree 1 for the pre-edge region and degree 2 for the post-edge region), conversion to k-space, truncation after AXAFS minimization, and background subtraction in k-space using a weighted (factor of 3) cubic-spline fit. The χ(k) function was weighted with k^3 prior to carrying out the Fourier transform. For both edges, the R-range used for fitting was between 1.0 and 4.5 Å. The range in k-space was 3–15 $Å^{-1}$.

Structural model development and fitting was carried out with the aid of several programs, including Atoms [21], FEFF [22], and FEFFIT [23]. Initially, a simple cubic model was attempted to fit the spectra with a mixing parameter, X_{mix}. This method led to very poor fits, even for the single oxide HfO_2 and ZrO_2 samples, and was therefore abandoned.

Previously reported XRD results [24] indicated that the samples exhibit a monoclinic structure. Therefore, the monoclinic structure of HfO_2 [25] was used as one set of input for the Atoms program [21], in order to position the atomic potentials in space: $a = 5.117$, $b = 5.175$, $c = 5.291$ with space group $p21/c$ and angles $\alpha = 90$, $\beta = 99.22$, and $\gamma = 90$, the output file of which essentially became the input file for FEFF [22], which was used to account for the main contributors to back-scattering by the nearest neighbor interactions. Only single scattering paths were considered in our model, as double scattering paths which are most important when the forward scattering angle is close to 180°, for our case, are deemed to contribute very little, although they are not negligible, as demonstrated by Li et al. [26]. Considering the Hf absorber in the binary oxide, the FEFF program [22] was executed twice, once with Hf as the absorber and Hf in the nearest metal coordination sphere, and a second time (implementing a separate subdirectory) with Hf as the absorber and Zr located in the nearest metal coordination sphere. In the same manner, FEFF [22] was carried out twice considering Zr as the absorber, to account for Hf–Zr in addition to Zr–Zr coordination. For ZrO_2, the monoclinic structure of ZrO_2 [25–27] was used as the input for the Atoms program [21], with parameters: $a = 5.150$, $b = 5.211$, $c = 5.317$, space group $p21/c$, and angles $\alpha = 90$, $\beta = 99.23$, and $\gamma = 90$. The FEFFIT program [23] was utilized to develop a structural model that could simultaneously fit both Hf L_{III} and Zr K edge data for the binary oxide catalysts with theoretical parameters to the experimental data, using a k^3 weighting during the fitting procedure to emphasize the first metal-metal coordination shell. In the model, with Hf as the absorber, a mixing parameter, X_{mix}, was applied to Zr in the nearest metal shell, while the balance $1 - X_{mix}$ was applied to Hf in the same shell. At the same time, with Zr as the absorber, the mixing parameter $1 - X_{mix}$ was applied to Hf in the nearest metal shell, while the balance, X_{mix}, was applied to Zr in the same shell. In this way, X_{mix} served as a global fitting parameter between the two data sets.

In fact, the monoclinic crystal structure is quite complex due to a lower degree of symmetry relative to the simple cubic structure, with 7 O atoms in the nearest oxygen shell, each residing at slightly different coordination distances, giving rise to a broad peak in the Fourier transform magnitude at low R, and 12 M atoms (where M = Hf or Zr) positioned at slightly different distances, with varying degree of degeneracy. Reasonable fits have been previously obtained for monoclinic structures by lumping certain path and fitting parameters together (e.g., zirconia [27, 28]). Although we attempted numerous fitting possibilities, based on previous literature studies, we opted for a well-reasoned approach in selecting certain parameters to be fixed or lumped together.

The model employed considers the seven oxygen atoms in the nearest coordination shell to be lumped into three separate coordinating subshells, resulting in 2 degeneracies at ~2.04 Å, 3 degeneracies at ~2.14 Å, and 2 degeneracies at ~2.24 Å. Likewise, as suggested in Table 1, similar coordination distances for Hf–M and Zr–M (M = Hf or Zr) in the nearest metal coordination sphere could be lumped together, resulting in 7 degeneracies at ~3.43 Å, 4 at ~3.94 Å, and 1 at ~4.53 Å, making use of an approach not unlike that undertaken by Li et al. [26] and Chadwick et al. [28] to successfully model monoclinic zirconia. The decision to use these ranges becomes obvious considering the theoretical values generated by FEFF as shown in Table 1. It is important to note that the actual values for the coordination numbers, N_{CN}, were fixed. S_0^2 was also fixed to 1.0 [26, 29], since as a variable, it is highly correlated with Δe_0, and also σ^2. The decision to use a value of 1.0 during fitting of the experimental data rather than 0.90 [26, 29] was that the resulting fits were slightly better with that choice. We chose to float Δe_0 for the single oxides, HfO_2 and ZrO_2, and then use the resulting values as set parameters for the mixed oxide catalysts. Otherwise, Δe_0 tended to float to nonsensical values. A similar approach for handling Δe_0 was used by Li et al. [26], who studied a variety of ZrO_2 materials with different crystal structures. On a per edge basis, the Debye-Waller factors for each M–O interaction (M = Zr or Hf) were lumped into one parameter to describe the first O shell and either 2 or 3 parameters to describe the M–M shell (M = Zr or Hf). The first covers the first 7 degeneracies and either 2 or 3 are

Table 1 Theoretical distances calculated by FEFF [22] and chosen lumped parameters for coordination distance, R

	Zr–O	Zr–Zr
m-ZrO_2	2.0352 ⇒ 1st O subshell	3.3052 ⇒ 1st Zr subshell
	2.0462	3.4185
	2.1351 ⇒ 2nd O subshell	3.4185
	2.1386	3.4375
	2.1585	3.4375
	2.2234 ⇒ 3rd O subshell	3.4456
	2.2479	3.5535
		3.8972 ⇒ 2nd Zr subshell
		3.8972
		3.9886
		3.9886
		4.5076 ⇒ 3rd Zr subshell
	Hf–O	Hf–Hf
m-HfO_2	2.0338 ⇒ 1st O subshell	3.3169 ⇒ 1st Hf subshell
	2.0697	3.4239
	2.1267 ⇒ 2nd O subshell	3.4239
	2.1392	3.4382
	2.1658	3.4382
	2.2270 ⇒ 3rd O subshell	3.4479
	2.2480	3.5643
		3.9081 ⇒ 2nd Hf subshell
		3.9081
		4.0010
		4.0010
		4.5271 ⇒ 3rd Hf subshell

used to describe the remaining 5 degeneracies. The reason is that the coordinating distances, while not the same, are very close. One would not anticipate that the degree of disorder to be so different solely due to the slight differences in atomic positions, R, for the different subshells within the entire broad shell. Furthermore, in this particular case, due to similarity in ionic radii, it was assumed that the Debye-Waller factor does not vary significantly due to substitution of Zr for Hf, and vice versa, either, resulting in an effective Debye-Waller factor that accounts for the presence of both Zr and Hf within each subshell. Although from a purely theoretical standpoint, it is important to consider the reduced mass for an interaction in determining Debye-Waller factors, we did not assign separate Debye-Waller factors for Zr–Zr, Zr–Hf, and Hf–Hf interactions within each subshell, we found empirically that this added too many parameters to the model, resulting in loss of physical meaning. Very reasonable values for the lumped σ^2 parameters for subshells were obtained using the above outlined model, which are reported as a weighted average for the entire shell (e.g., 12 total interactions for the broad shell for Hf–M, with 7 interactions for the 1st subshell, 4 for the 2nd subshell, and 1 for the 3rd subshell).

2.4 Reaction Testing

Catalytic testing was carried out using a tubular fixed bed reactor. The catalyst was activated at 500 °C in hydrogen for 4 h prior to testing. Alcohol was pumped at a rate to give a space velocity of 0.4 LHSV. Liquid products were collected at hourly intervals and analyzed for conversion and alkene distribution using gas chromatography. A normal catalytic run lasted for 5–8 h. Conversion levels varied from 2 to 20% conversion of the alcohol. The maximum activity was obtained with the $Hf_{0.20}Zr_{0.80}O_2$ solid solution.

3 Results and Discussion

3.1 XPS

The normalized XPS spectra for the Hf 4f and Zr 3d ionizations are presented in Fig. 1. As shown in Table 2, the surface shell atomic ratios of Zr/(Zr + Hf) were found to be close to their bulk ratios. The only exception was the $Hf_{0.05}Zr_{0.95}O_2$ solid solution, which was somewhat lower, at 0.80. Because the X-ray energy is 1273 eV and binding energies are ~20 and ~185 eV, respectively, the kinetic energies of photoelectrons will be in the range of 1080–1253 eV. The mean free path of electrons in elemental solids depends on kinetic energy. When kinetic energy is less than 1000 eV, penetration depth is ~1–2 nm. Thus, at these conditions, layers beneath the surface will also contribute to the signal, and this is why we use the term "surface shell" to describe the XPS results. It is important to note that previous results of other surface techniques (e.g., Raman spectroscopy [16] and ISS [15]) are consistent with the XPS concentrations obtained in this work.

3.2 Extended X-ray Absorption Fine Structure Spectroscopy

The decision to carry out fitting of EXAFS data was made after, on a theoretical basis, considering the impact of atomic substitution of Hf in the first metal coordination shell of hafnia by Zr. These theoretical models are displayed in Fig. 2. The k^3-weighted $\chi(k)$ vs. k and Fourier transform magnitudes are presented for theoretical perfect solid solutions of monoclinic HfO_2, $Hf_{0.50}Zr_{0.50}O_2$, and $Hf_{0.05}Zr_{0.95}O_2$, respectively. R values for O, Hf, and Zr were fixed to their nominal values, Debye-Waller factors σ^2 were set to zero, S_0^2 was set to 0.90 [26, 29], and Δe_0 was fixed at 8 eV. Theoretical spectra were generated using the FEFF [22] and FEFFIT [23] programs. For HfO_2, the peaks for Hf–Hf

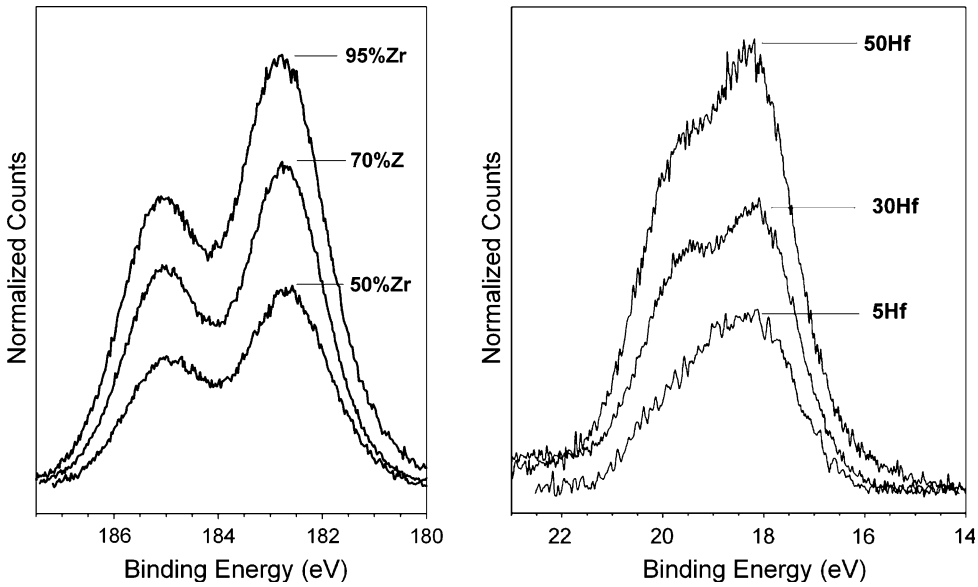

Fig. 1 (*Left*) Zr 3d XPS spectra for the binary oxides including, moving upward, $Hf_{0.50}Zr_{0.50}O_2$, $Hf_{0.30}Zr_{0.70}O_2$, and $Hf_{0.05}Zr_{0.95}O_2$, and (*Right*) Hf 4f XPS spectra for the binary oxides including, moving upward, $Hf_{0.05}Zr_{0.95}O_2$, $Hf_{0.30}Zr_{0.70}O_2$, and $Hf_{0.50}Zr_{0.50}O_2$

Table 2 Zr/(Hf + Zr) surface atomic concentration ratios obtained from XPS by application of Scofield factors [18]

Catalyst description	Binding energy shift (eV)	Zr/(Zr + Hf)
$Hf_{0.05}Zr_{0.95}O_2$	8.875	0.80
$Hf_{0.30}Zr_{0.70}O_2$	8.275	0.67
$Hf_{0.50}Zr_{0.50}O_2$	8.875	0.47

coordination are readily apparent. However, there is an important destructive interference of waveforms for the Hf–Zr and Hf–Hf contributions from the first metal shell in the case of the $Hf_{0.50}Zr_{0.50}O_2$ catalyst. For the case where the concentration of Zr is high enough such that it accounts for 95% of the atoms in the first metal coordination shell, sharp peaks again arise in the Fourier transform magnitude spectra, as Hf–Zr coordination is favored. From this preliminary evaluation, it would appear then that important information on the extent of mixing between Hf and Zr may be obtained from EXAFS fitting procedures.

It is therefore interesting in the case of Hf and Zr to determine if the surface ratios extend into the bulk of the sample, and whether or not EXAFS can provide some verification of the degree of mixing between the two metal oxide components in the binary mixed solid solution. The k^3-weighted $\chi(k)$ functions, their Fourier Transform magnitudes, and the theoretical results of the model from the simultaneous nonlinear least squares fitting routine, are presented in Table 3 and Fig. 3. The experimental k^3 weighting was used to emphasize the contribution of the higher Z elements. For the HfO_2 single oxide, the backscattering amplitude envelope in the weighted $\chi(k)$ function arising from Hf–Hf coordination is very evident. However, replacing close to half of the atoms of Hf by Zr in the Hf–M (again, M = Zr or Hf) coordination shell results in considerable annihilation of the waveform, since the oscillations arising from Hf–Hf and Hf–Zr coordination are slightly offset from one another. Interference phenomena due to atom substitution were previously reported during EXAFS investigations of Pt–Sn alloys [30], where the presence of both metallic Pt and Pt–Sn bimetallic clusters led to the appearance of a new peak in the FT magnitude spectrum due to interference of the Pt–Pt from Pt^0 clusters and Pt–Sn from the clusters exhibiting the alloy. More recently, another poignant reminder regarding interference phenomena was reported in the case of mixed-phase zirconia materials containing both the tetragonal and monoclinic phases [31]. In that instance, the Zr–Zr peak was found to decrease due to cancellation effects in $\chi(k)$ due to variations between the monoclinic and tetragonal zirconia waveforms [31], reminding people to pay attention to mixed phase cancellation effects. Regarding Hf L_{III} edge data, in our case, as Zr content is increased, there appears to be considerable destructive interference between the waveforms in $\chi(k)$ arising from the Hf–Hf and Hf–Zr contributions at 50% Zr content, as the envelope is markedly attenuated. Yet, at higher levels of Zr addition (0.70 Zr and 0.95 Zr), the signal for Hf–Zr becomes apparent and predominant in the high k region of $\chi(k)$. The result in the Fourier transform magnitude is a slight decrease in the peak position in R-space for Hf–M from one extreme, purely Hf–Hf coordination for the HfO_2 sample, to the other, predominantly Hf–Zr coordination for the $Hf_{0.05}Zr_{0.95}O_2$ catalyst sample, in line with the theoretical predictions depicted in Fig. 2.

The sensitivity of the backscattering functions and therefore, the $k^3 \cong \chi(k)$ signal, to atom type, especially in the amplitude component of the EXAFS equation, $A_j(k)$, is

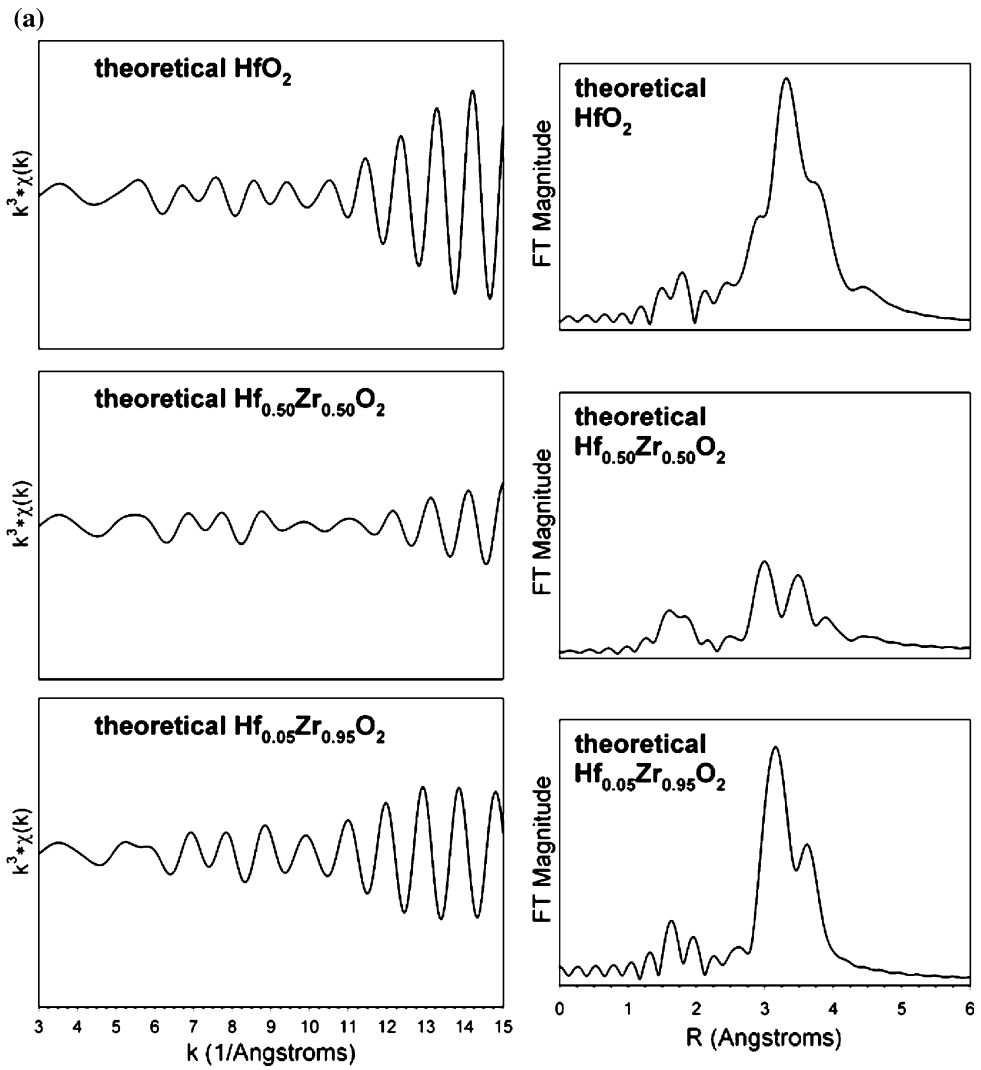

Fig. 2 **a** k^3-weighted χ(k) vs. k (*left*) and Fourier transform magnitudes (*right*) for theoretical perfect solid solutions for, moving downward, monoclinic (a) HfO_2, (b) $Hf_{0.50}Zr_{0.50}O_2$, and (c) $Hf_{0.05}Zr_{0.95}O_2$. R values for O, Hf, and Zr were fixed to nominal values, σ^2 set to zero, S_0^2 set to 0.90, and Δe_0 was fixed at 8 eV. Theoretical spectra (Hf L_{III} edge) were generated using Feff [22] and Feffit [23]. Note the destructive interference of waveforms in χ(k) for Zr and Hf in the first metal shell for the $Hf_{0.50}Zr_{0.50}O_2$ case, and the resulting diminishing of the Fourier transform magnitude for Hf–M (M = Hf, Zr) coordination. **b** k^3-weighted χ(k) vs. k (*left*) and Fourier transform magnitudes (*right*) for theoretical perfect solid solutions for, moving downward, monoclinic (a) ZrO_2, (b) $Zr_{0.70}Hf_{0.30}O_2$, and (c) $Zr_{0.50}Hf_{0.50}O_2$. R values for O, Hf, and Zr were fixed to nominal values, σ^2 set to zero, S_0^2 set to 0.90, and Δe_0 was fixed at 5.5 eV. The theoretical spectra (Zr K edge) were generated using Feff [22] and Feffit [23]. Although some changes are observed, in comparison with the Hf L_{III} theoretical spectra (**a**), the theoretical spectra for the Zr K edge appear to be less sensitive to the mixing effect

exhibited by comparison of the spectra of HfO_2 (essentially all Hf–Hf coordination in the nearest metal shell) with $Hf_{0.05}Zr_{0.95}O_2$ (high degree of Hf–Zr coordination in the closest metal shell). The envelope displays a larger amplitude for hafnia in the high k region, as expected from the theoretical predictive models shown in Fig. 2.

The results taken at the Zr K edge (Fig. 4) complemented Hf L_{III} edge results, allowing for a more accurate determination of X_{mix} during simultaneous fitting of data acquired at the two edges with the global theoretical structural model. The uncertainty in X_{mix} was approximately ±0.05. Including the additional data set essentially removed one degree of freedom from the fitting relative to a model in which the two edges would be fitted independently. That is, X_{mix} was constrained by both data sets as a global fitting parameter, resulting in an interdependent model. Relying on data from both two edges, fit at the same time, it appears that EXAFS could continue to gain in importance as a useful tool in verifying whether, and determining the extent to which, solid solutions are formed during catalyst preparation, especially considering recent trends toward more complex, multi-component oxides (e.g., see [32]).

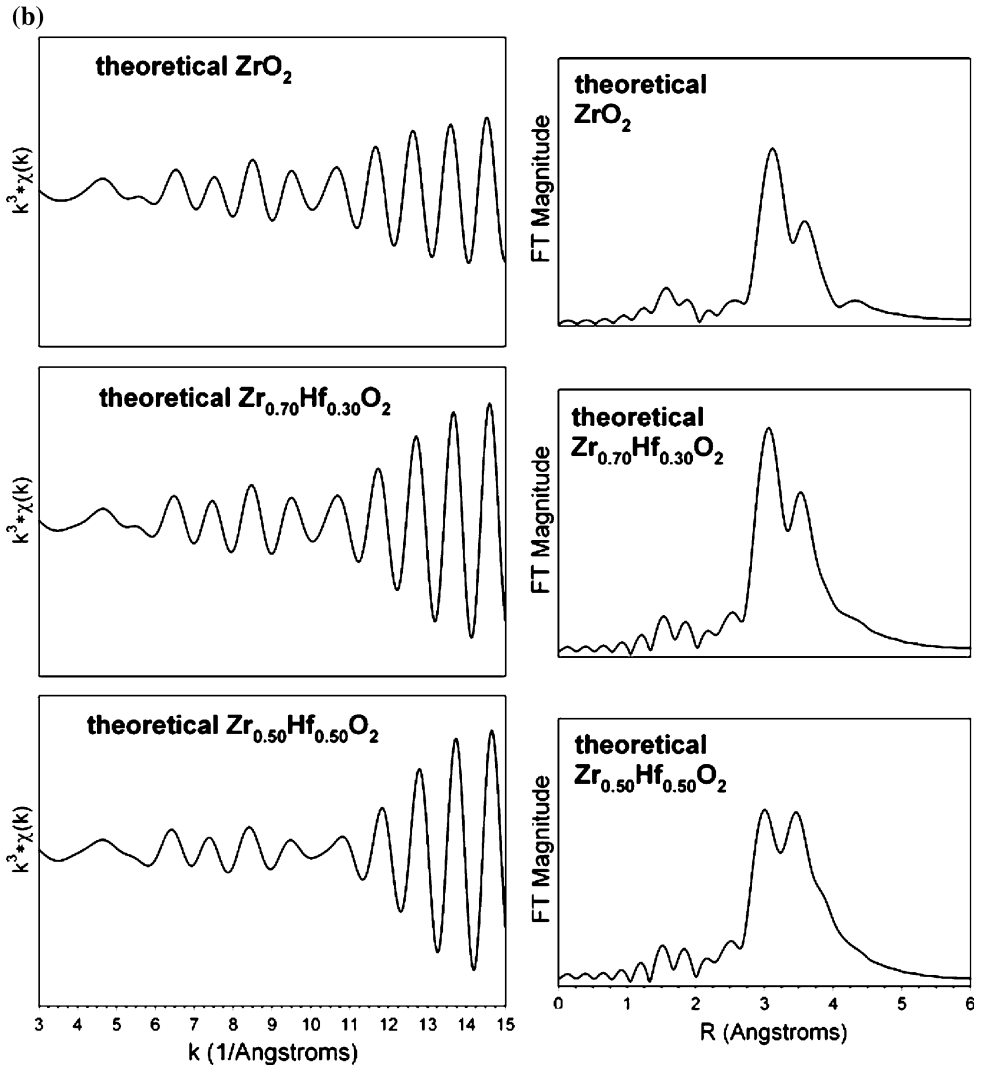

Fig. 2 continued

Comparing the X_{mix} values among the binary oxide catalysts, the results are quite consistent with their nominal bulk values if the solids formed near-perfect solid solutions on a localized (i.e., atomic) level. Again, as with the XPS results, the $Hf_{0.05}Zr_{0.95}O_2$ sample resulted in a lower than nominal value for Hf–Zr coordination, with about 76.4% of the M atoms on average coordinated to Zr instead of 95%. However, the result was consistent with the surface shell concentration value obtained from XPS of 80%. Nevertheless, the results of both XPS and EXAFS suggest that Hf and Zr form a nearly perfect solid solution $Hf_XZr_{1-X}O_2$ over a wide range of X. Moreover, this system appears to be one case in which the surface shell (i.e., including some subsurface layers by XPS) and surface (i.e., by Raman [16] and ISS [15]) concentrations are virtually identical with the bulk compositions, indicating that the surface layer is not enriched with one particular element over another. That is, the surface shell and surface compositions of Hf relative to Zr can be considered to be directly extrapolated from the bulk monoclinic crystal structure.

Another interesting extrapolation from the data is a comparison between the binding energy shift from XPS, and the edge energy e_0 shift calculated during EXAFS fitting [33], which are related. Comparing the shifts in e_0 resulting from EXAFS modeling (Table 3) with the binding energy shifts from XPS (Table 2), there appears to be good agreement between the values, which are both on the order of +8 to 9 eV for hafnia. The uncertainty in Δe_0 calculated from fitting the EXAFS region with FEFFIT for HfO_2 and ZrO_2 was $\sim$1–2 eV. The positive value is not surprising considering both the chemical shift due to oxidation state as well as the shift due to charging of the insulator. Interestingly, the energy shifts appear to be generally consistent between the two characterization techniques.

Table 3 Simultaneous fitting model using data reported at both Hf L_{III} and Zr K edges, and lumped fitting parameters for R and σ^2, which is reported as a weighted average for the entire broad shell

Catalyst	Δe_0 (eV)	R (Å)	N_{CN}	σ^2 (Å^2)	R (Å)	N_{CN}	σ^2 (Å^2)	X_{mix}	ρ (%)
	Hf–O				Hf–M, where M is equal to Hf or Zr, and X_{mix} is the fraction of M that is Zr				
HfO_2	8.6	2.11	2.0	0.0082	3.44	7.0	0.0060	–	5
		2.11	3.0		3.99	4.0			
		2.25	2.0		4.54	1.0			
$Hf_{0.50}Zr_{0.50}O_2$	Set	2.04	2.0	0.0029	3.44	7.0	0.0058	52.3	23
		2.14	3.0		4.00	4.0			
		2.25	2.0		4.53	1.0			
$Hf_{0.30}Zr_{0.70}O_2$	Set	2.04	2.0	0.0028	3.45	7.0	0.0090	70.5	13
		2.14	3.0		3.93	4.0			
		2.25	2.0		4.55	1.0			
$Hf_{0.05}Zr_{0.95}O_2$	Set	2.04	2.0	0.0030	3.44	7.0	0.0069	76.4	10
		2.14	3.0		3.93	4.0			
		2.25	2.0		4.55	1.0			
	Zr–O				Zr–M, where M is equal to Zr or Hf, and X_{mix} is the fraction of M that is Hf				
ZrO_2	5.4	2.09	2.0	0.0073	3.46	7.0	0.0087	–	7
		2.12	3.0		3.98	4.0			
		2.25	2.0		4.54	1.0			
$Zr_{0.95}Hf_{0.05}O_2$	Set	2.04	2.0	0.0030	3.49	7.0	0.0069	23.6	10
		2.14	3.0		3.97	4.0			
		2.25	2.0		4.58	1.0			
$Zr_{0.70}Hf_{0.30}O_2$	Set	2.03	2.0	0.0028	3.51	7.0	0.0090	29.5	13
		2.14	3.0		3.97	4.0			
		2.25	2.0		4.58	1.0			
$Zr_{0.50}Hf_{0.50}O_2$	Set	2.04	2.0	0.0029	3.45	7.0	0.0058	47.7	23
		2.14	3.0		3.79	4.0			
		2.25	2.0		4.12	1.0			

The edge energy shift, Δe_0, was floated for the single oxides, and for the mixed binary oxide catalysts, fixed to the single oxide values. The mixing parameter, X_{mix}, was also floated. The amplitude reduction factor, S_0^2 was fixed to a value of 1.0. Coordination numbers for subshells of oxygen and metal were also fixed

3.3 Reaction Testing

The dramatic change in dehydration selectivity is reported in Fig. 5. On the left, a comparison is shown between solid solution catalysts, and those prepared by doping the surface of zirconia with hafnia. In either case, a step change in product selectivity occurs at a molar percentage of 75% Zr for the solid solutions (characterized in this work), and 90% Zr for the hafnia doped zirconia series. In a similar manner, in Fig. 5 (right), for the hafnia-doped zirconia series, there is a virtually identical step change increase at 90% Zr for dehydration selectivity of butanol. The remarkable change in product selectivity therefore appears to be only indirectly influenced by the changing composition of Hf and Zr on the catalyst surface. Otherwise, one would expect a gradual change in selectivity, allowing one to tune the products of interest by adjusting the atomic ratio Hf/Zr, at the surface.

In considering the history of alcohol conversion, the reviews of Mars et al. are essential [34, 35]. Eucken [36] proposed a correlation between the selectivity and the quantity: $\eta = (\text{cation radius})^3 \Big/ [(\text{molar volume percation})(\text{valency})]$ Empirically, dehydration was found to be favored if the cation radius was larger, and the valency smaller, resulting in a large value for η (e.g., TiO_2, SiO_2, and Al_2O_3). On the other hand, dehydrogenation was found to be promoted by a small cation and a high valency (e.g., MgO, ZnO). Wicke [37] indicated that a small cation surrounds itself almost completely by oxygen ions, and suggested that this never happens to the same extent when the cation is large.

To link the selectivity with the structure based on this simple model, the following mechanisms were envisioned:

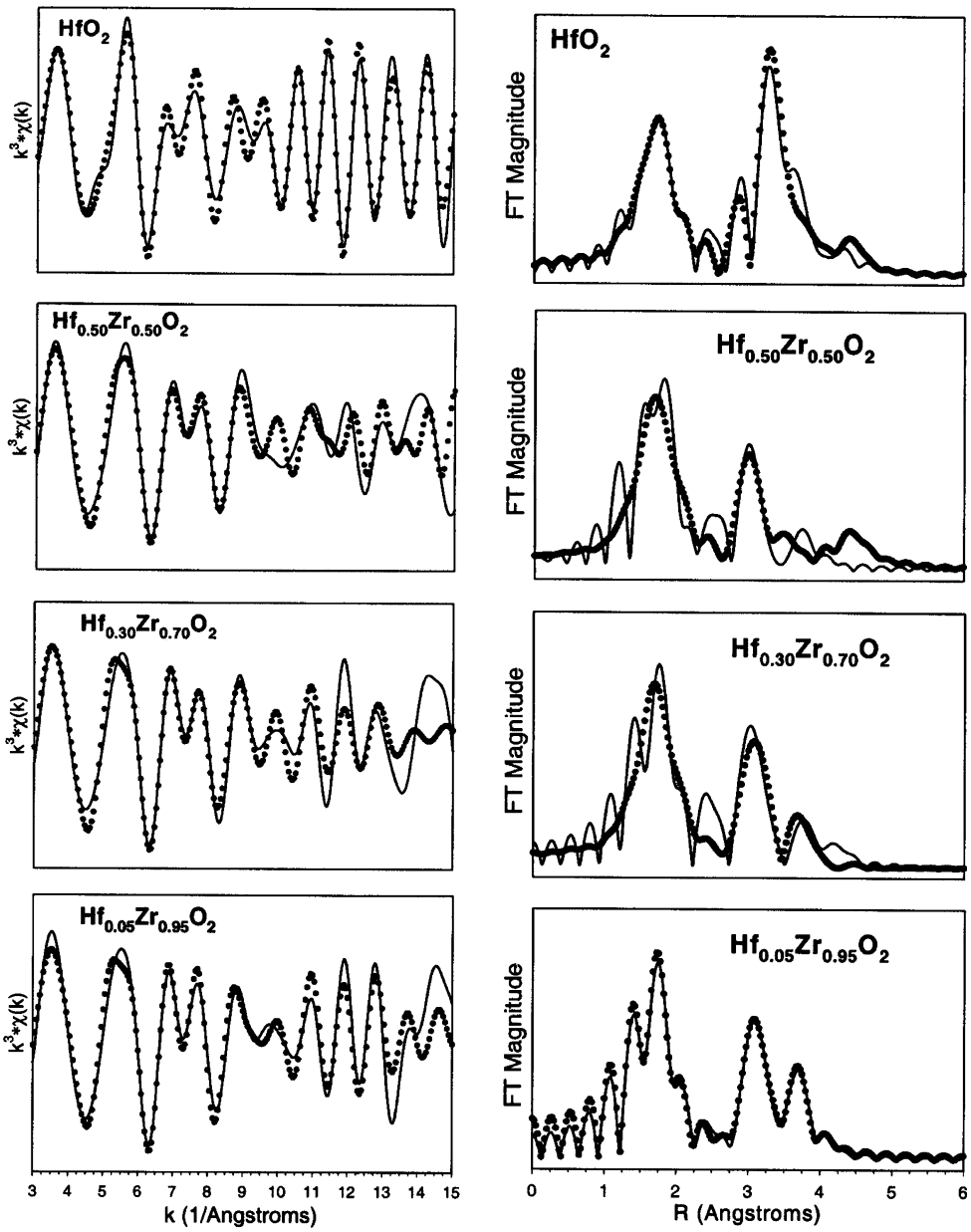

Fig. 3 k^3-weighted $\chi(k)$ vs. k (*left*) and Fourier transform magnitudes (*right*) for experimental data (*solid lines*) and theoretical model best fits (*filled circles*) for, moving downward, monoclinic (a) HfO_2, (b) $Hf_{0.50}Zr_{0.50}O_2$, (c) $Hf_{0.30}Zr_{0.70}O_2$, (d) $Hf_{0.05}Zr_{0.95}O_2$. Data recorded at the Hf L_{III} edge

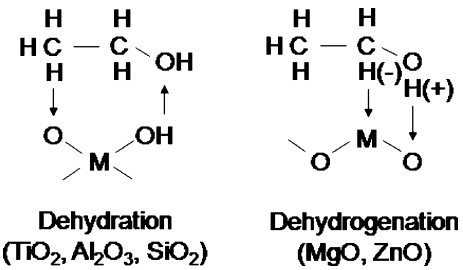

Following this line of reasoning, Mars [34] indicated that the picture suggested two important points: (1) there should exist a correlation between activation energy of dehydration and the bonding energy of the proton (i.e., Bronsted acidity) and (2) if an oxide tended to lose water at the surface, the number of acid sites would be reduced, such that the oxide should favor the dehydrogenation route. The latter was supported by the fact that MgO tended to lose water at relatively low temperatures.

With these concepts regarding selectivity for dehydrogenation and dehydration in mind, and returning to the Hf–Zr mixed oxides, can an adequate explanation be provided to explain (1) the difference in selectivity between HfO_2 and ZrO_2, and (2) the step change in selectivity for the series of mixed oxides, which favors dehydration for the high Zr-content materials?

Application of the initial relationship of Eucken to fully oxidized hafnia and zirconia results cannot adequately

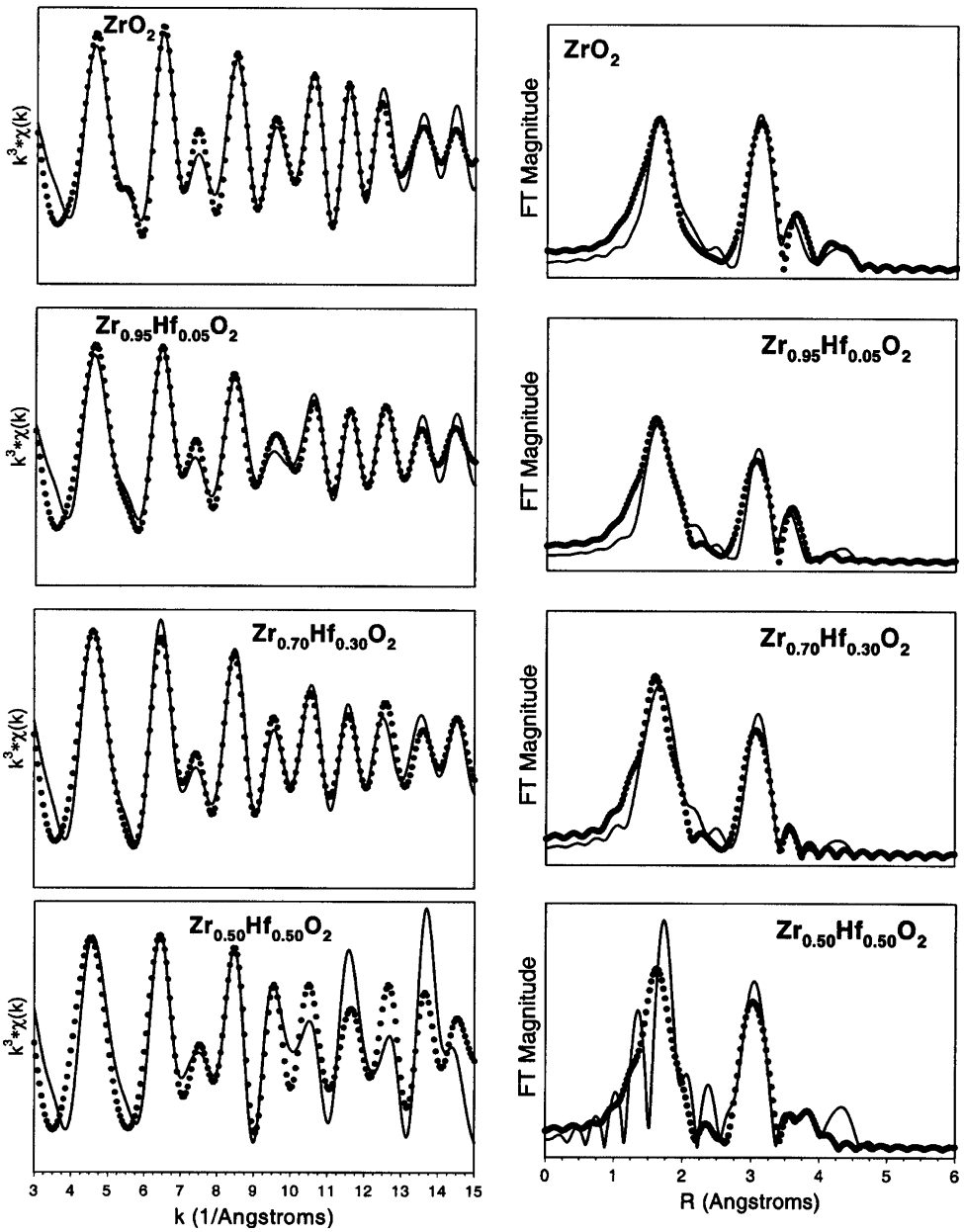

Fig. 4 k^3-weighted $\chi(k)$ vs. k (*left*) and Fourier transform magnitudes (*right*) for experimental data (*solid lines*) and theoretical model best fits (*filled circles*) for, moving downward, monoclinic (a) ZrO_2, (b) $Zr_{0.95}Hf_{0.05}O_2$, (c) $Zr_{0.90}Zr_{0.30}O_2$, (d) $Hf_{0.50}Zr_{0.50}O_2$. Data recorded at the Zr K-edge

explain the selectivity difference. The ionic radii (72 pm for zirconia and 71 pm for hafnia), the crystal structures (see previous crystallographic data), and the valences (both +4) are virtually identical, and these are the input parameters for η.

Therefore, it would appear, especially as the oxides were activated at high temperature (>450), that the catalytic phenomena be a result of the number of defects (i.e., O deficiencies or bridging OH groups) at the surface. According to Mars, the oxides which more easily lost water at low temperature favored dehydrogenation. Said another way, dehydration selectivity appears to be favored over oxides which retain stoichiometric O at the surface, while dehydrogenation appears to be favored over oxides which more easily produce defects (O vacancies or their related Type II bridging OH groups). According to this model, it is suggested that the HfO_2-rich mixtures may offer a more facile ability to generate these surface defects over ZrO_2. It is important to consider that such defect-laden materials would tend to favor the activation of molecules such as steam, formic acid, and alcohols by dissociative adsorption.

However, the situation with zirconia and hafnia appear to be different than expected from the above discussion. For zirconia, activation in air or oxygen produces a material that has about equal selectivity for dehydration and dehydrogenation of 2-octanol [38]. Furthermore, the oxygen pretreated sample was unselective for 1-octene formation and about equal amounts of the 1-, *cis*-2- and

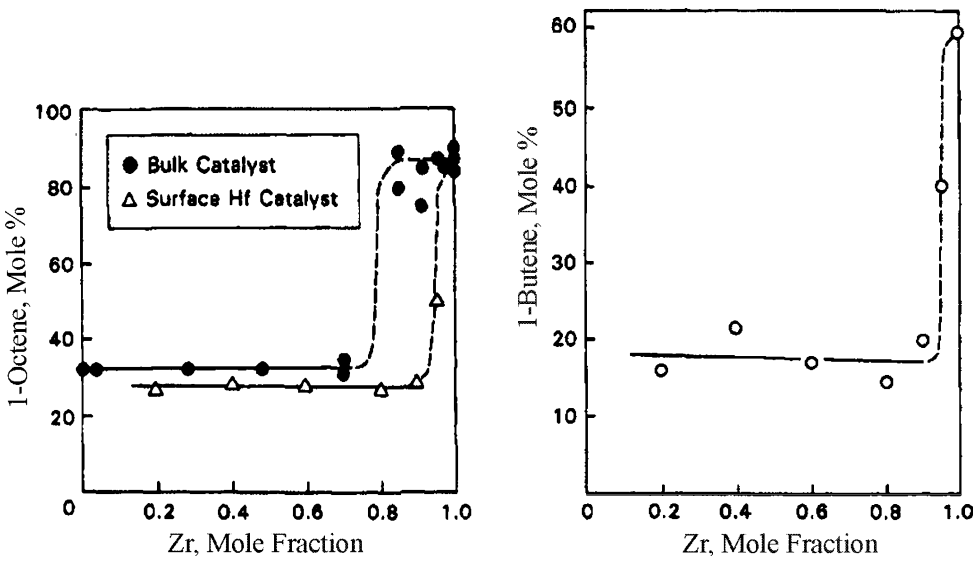

Fig. 5 (*Left*) The fraction of 1-octene present in 2-octanol conversion products, indicating dehydration selectivity for (*closed circles*) the solid solution catalysts and (*open triangles*) the hafnia-doped zirconia catalysts. (*Right*) The fraction of 1-butene present in 2-butanol conversion products, indicating dehydration selectivity for the hafnia-doped zirconia catalysts. Note the step change in product selectivity [16]

trans-2-octenes were produced while the hydrogen pretreated sample produced about 90% of the 1-octene isomer. Thus, it appears that with zirconia, the catalytic activity that is selective for alcohol dehydration and the production of 1-alkene from a 2-alcohol resides in the oxygen vacant sites generated by the hydrogen pretreatment.

Hafnia differs from zirconia in that both the air and the hydrogen pretreated samples have similar catalytic properties. Hafnia following either a hydrogen or oxygen pretreatment was a selective dehydration catalyst, usually with 95% or more of the conversion being dehydration. In spite of the very selective dehydration properties, about equal amounts of the 1-, *cis*-2- and *trans*-2-octene isomers were obtained. If the inference from the zirconia case that the 1-octene selectivity resides in the oxygen vacancy sites, then it is very much more difficult to generate these oxygen deficient sites on hafnia than on zirconia.

In the case of the mixed oxides, whether the bulk oxide or the surface-only mixed oxide catalyst, the alkene selectivity of the samples resemble hafnia until at least 80% of the mixed bulk or the mixed surface phase is zirconia. The alcohol conversion, surface area, crystal phase, and crystallite size determined by XRD line broadening and TEM measurements are given in reference 15. When the dominant fraction of the mixed oxide is zirconium, the catalytic properties then resemble that of zirconia. It therefore appears that when the Zr fraction is below 80%, the surface properties resemble that of pure hafnia but when the Zr fraction exceeds about 80% the surface properties resemble that of pure zirconia. This step change in catalytic properties does not appear to follow any of the properties associated with surface or bulk compositions that have been examined in this and our earlier studies [15, 16].

4 Conclusions

Binary oxides of the type $Hf_XZr_{1-X}O_2$ were prepared according to a recipe that yields the monoclinic structure, and characterized by EXAFS spectroscopy. A simultaneous fitting model was tested that fits data from both edges at the same time, making use of an interdependent mixing parameter X_{mix} to take into account substitution of the complementary atom in the nearest metal-metal shell. EXAFS results suggested that a solid bulk solution was formed over a wide range of X for $Hf_XZr_{1-X}O_2$ the binary oxides, and XPS confirmed that the relative ratio was retained in the surface shell. The concentrations obtained by XPS were consistent with our earlier surface characterization results of Raman and ISS spectroscopies. Interestingly, although the cation radius, crystal properties, and valencies were similar for pure oxides, hafnia favored dehydrogenation and zirconia favored dehydration, thereby breaking classical correlations of selectivity and cation size, valency. Also, for the mixed oxides, the increase in selectivity for dehydration of alcohols at high Zr content did not correlate smoothly with the tuned relative atomic concentration of Hf to Zr. The step change in selectivity at high Zr content appears to be due to other indirect factors (e.g., surface defects, oxygen vacancies).

References

1. Vlaic G, Fornasiero P, Geremia S, Kaspar J, Graziani M (1997) J Catal 168:386
2. Nagai Y, Yamamoto T, Tanaka T, Yoshida S, Nonaka T, Okamoto T, Suda A, Sugiura M (2001) J Synchrotron Radiat 8:616

3. Balducci G, Saiful Islam M, Kaspar J, Fornasiero P, Graziani M (2000) Chem Mater 12:677
4. Fornasiero P, Balducci G, Di Monte R, Kaspar J, Sergo V, Gubitosa G, Ferrero A, Graziani MJ (1996) J Catal 164:173
5. Gonzalez-Velasco JR, Gutierrez-Ortiz MA, Marc JL, Botas JA, Gonzalez-Marcos MP, Blanchard G (1999) Appl Catal B: Environ 22:167
6. Bunluesin T, Gorte R, Graham G (1998) Appl Catal B 15:107
7. Ricote S, Jacobs G, Milling M, Ji Y, Patterson PM, Davis BH (2006) Appl Catal A: Gen 303:35
8. Alifanti M, Baps B, Delmon B, Bernard (2004) Prog Catal 13:43
9. Hirata T, Asari E, Kitajima M (1994) J Solid State Chem 110:201
10. Trovarelli A (ed) (2002) Catalysis by ceria and related materials. Imperial College Press, London
11. Zheng W, Bowen KH Jr, Li J, Dabkowska I, Gutowski M (2005) J Phys Chem A 109:11521
12. Overbury SH, Huntley DR, Mullins DR, Glavee GN (1998) Catal Lett 51:133
13. Kim T, Vohs JM, Gorte RJ (in press) Ind Eng Chem Res
14. Lide DL (ed) (2001–2002) Handbook of chemistry and physics, 82nd edn. CRC, Boca Raton, FL
15. Davis BH (1984) Appl Surf Sci 19:2000
16. Simpson S, Davis BH (1987) J Phys Chem 91:5664
17. Freeman GB, Collins DJ, Waters JC, Davis BH (1980) J Phys Chem 84:55
18. Scofield JH (1976) J Electron Spectrosc Relat Phenom 8:129
19. Jacobs G, Chaney JA, Patterson PM, Das TK, Maillot JC, Davis BH (2004) J Synchrotron Radiat 11:414
20. Ressler T (1998) J Synchrotron Radiat 5:118
21. Ravel B (2001) J Synchrotron Radiat 8:314
22. Rehr JJ, Zabinsky SI, Albers RC (1992) Phys Rev Lett 69:3397
23. Newville M, Ravel B, Haskel D, Stern EA, Yacoby Y (2005) Physica B 208–209:154
24. Zhao X, Vanderbilt D (2002) Phys Rev B 65:233106-1
25. Hirata T (1994) Phys Rev B 50:2874
26. Li P, Chen I-W, Penner-Hahn JE (1993) Phys Rev B 48:10063
27. Zhao X, Vanderbilt D (2002) Phys Rev B 65:075105-1
28. Chadwick AV, Pooley MJ, Rammutla KE, Savin SLP, Rougier A (2003) J Phys Condens Matter 15:431
29. Ravel B (2001) EXAFS analysis using FEFF and FEFFIT workshop, 27–29 June 2001. National Synchrotron Light Source, Brookhaven National Laboratory, Upton, NY, USA
30. Borgna A, Stagg-Williams SM, Resasco DE (1998) J Phys Chem B 102:5077
31. Yang P, Cai X, Xie Y, Xie Y, Hu T, Zhang J, Liu T (2003) J Phys Chem B 107:6511
32. Adachi G, Imanaka N, Kang ZC (eds) (2004) Binary rare earth oxides. Kluwer Acad. Pub., London, England
33. Englisch M, Lercher JA, Haller GL (1996) In: Iwasawa Y (ed) X-ray absorption fine structure for catalysts and surfaces, chapter 8. World Scientific Publishing Co., Singapore
34. Mars P (1959) In: de Boer JH et al (eds) Proceedings of the symposium on the mechanism of heterogeneous catalysis. Elsevier Publishing Company, Amsterdam, The Netherlands
35. Mars P, Scholten JJF, Zwietering P (1963) Adv Catal 14:35
36. Eucken A (1949) Naturwissenschaften 36:48
37. Wicke E (1949) Z Elektrochem 53:279
38. Davis BH, Ganesan P (1979) Ind Eng Chem Prod Res Dev 18:191